

RSC Advances



This is an *Accepted Manuscript*, which has been through the Royal Society of Chemistry peer review process and has been accepted for publication.

Accepted Manuscripts are published online shortly after acceptance, before technical editing, formatting and proof reading. Using this free service, authors can make their results available to the community, in citable form, before we publish the edited article. This *Accepted Manuscript* will be replaced by the edited, formatted and paginated article as soon as this is available.

You can find more information about *Accepted Manuscripts* in the [Information for Authors](#).

Please note that technical editing may introduce minor changes to the text and/or graphics, which may alter content. The journal's standard [Terms & Conditions](#) and the [Ethical guidelines](#) still apply. In no event shall the Royal Society of Chemistry be held responsible for any errors or omissions in this *Accepted Manuscript* or any consequences arising from the use of any information it contains.

Cite this: DOI: 10.1039/c0xx00000x

www.rsc.org/xxxxxx

ARTICLE TYPE

Theoretical insights into copper(I)-NHC-catalyzed C-H carboxylation of terminal alkynes with CO₂: the reaction mechanisms and the roles of NHC

Longhua Yang^{a,b}, Yanli Yuan, Hongming Wang^{*a}, Ning Zhang^{*b} and Sanguo Hong^b

⁵ Received (in XXX, XXX) Xth XXXXXXXXX 20XX, Accepted Xth XXXXXXXXX 20XX
DOI: 10.1039/b000000x

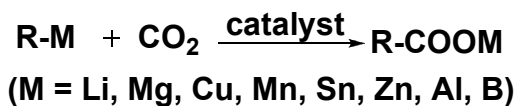
The reaction mechanisms of copper(I)-NHC-catalyzed C-H carboxylation of terminal alkynes with CO₂ had been investigated by DFT calculations (NHC=N-heterocyclic carbene). Three types of reaction mechanisms were designed, explored and compared. The optimal reaction channels of corresponding pathways were selected out. It was investigated that the formation of new C-C bond in the insertion process of activated CO₂ by NHC was induced by the formation of Cu-O bond. Also, the functions of NHC were figured out. Our calculations investigated that (1) the special difunctional roles of NHC can indeed facilitate the reaction process after the formation of CO₂-NHC-Cu cocatalyst, while the unexpected low energy of this cocatalyst results in its ultrastability, and then hinders the dropping of energy barrier in the whole reaction. (2) The additional interaction of NHC to the same metal atom will promote the insertion process of CO₂ through increasing the electrophilic of the metal center.

1. INTRODUCTION

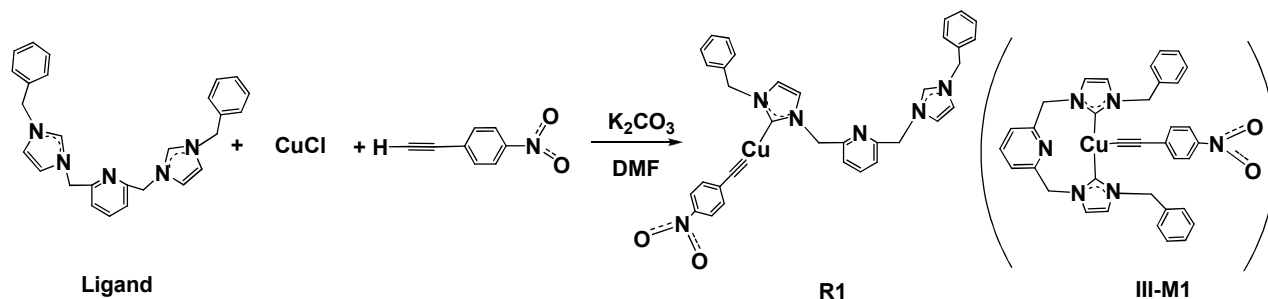
The chemical capture, conversion and fixation of carbon dioxide have attracted much attention due to global warming.¹⁻³ As an environmentally friendly feedstock, utilizing CO₂ for organic synthesis is a highly attractive approach to making commodity chemicals to address the energy penalty problem.^{16,4} However, developing more efficient catalyst to incorporate CO₂ into organic molecules under mild conditions remains a great challenge in real world applications.⁵

Carboxylic acids, as one of the most important types of compounds in medicinal chemistry, numerous protocols had been well-established.⁶⁻⁷ One of the most attractive and straightforward reactions is the direct catalytic carboxylation of organic compounds with CO₂.⁸⁻¹⁶ The essence of this method is the direct carboxylation of carbon nucleophiles using CO₂ as the

electrophile.⁶ Typically, organometallic reagents are taken as precursors universally, such as organolithium. But this method is always limited by the low catalytic performances, harsh reaction conditions, and restricted substrate scope. (Scheme 1) Although some transition-metal-catalyzed carboxylations of less reactive carbon have an improving performance in functional group tolerance, such as organotin¹⁶, organoboron¹⁰, organozinc¹⁵, the stoichiometric consumption is still a disadvantage.



⁴⁰ Scheme 1. The reaction equation of organometallic reagents and CO₂ for carboxylation.



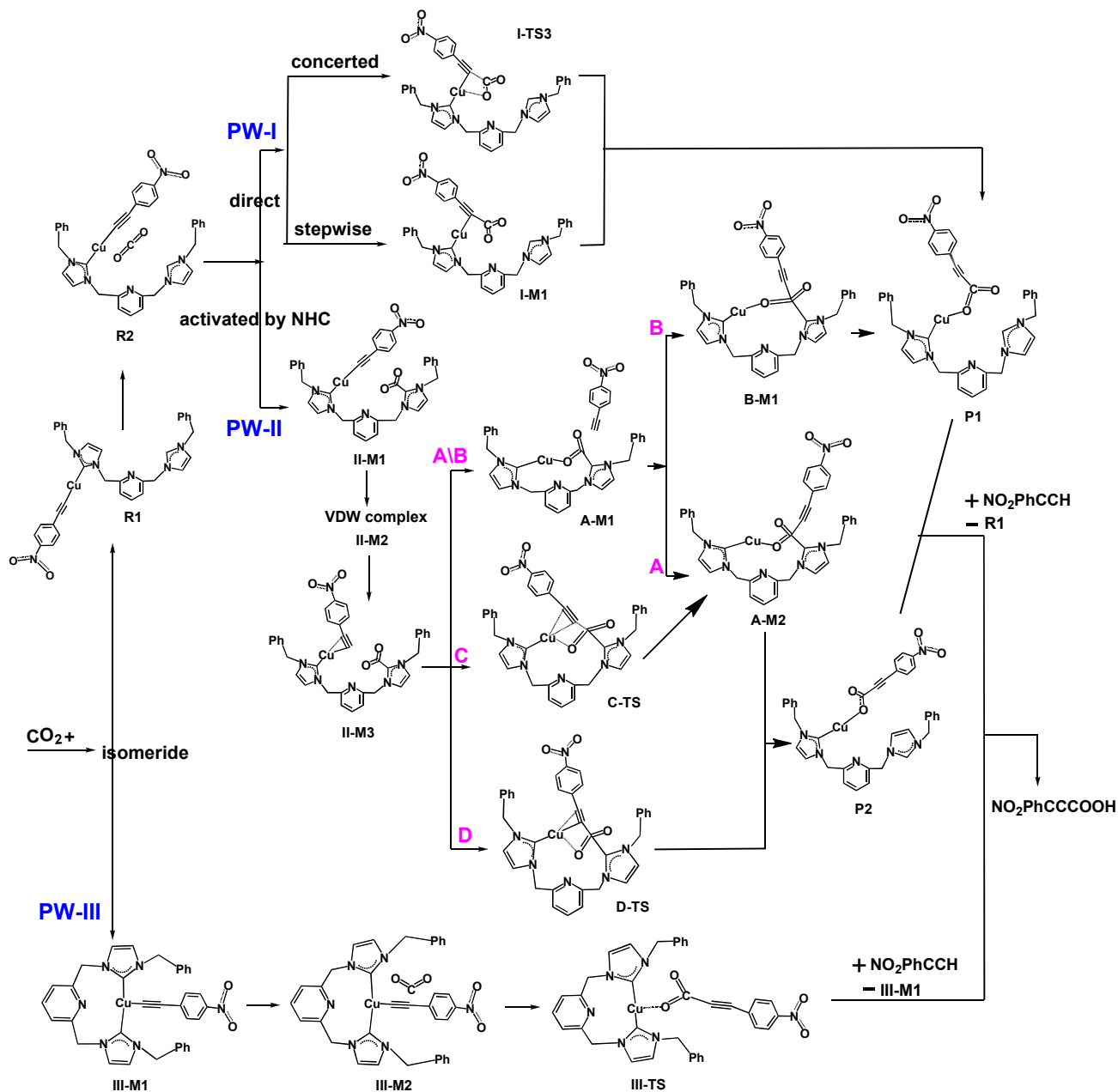
Scheme 2. The equation of the generations of R1 and III1.

⁴⁵ Recently, other economical methods have been reported by direct C-H bond activation and carboxylation with CO₂.^{8,17-21} For

instance, Nolan's group reported the carboxylation of C-H bonds of highly activated arenes and heterocycles using NHC-gold(I)

and NHC-copper(I) complexes to catalyze CO_2 .^{17,18} Gooßen's group reported the C-H carboxylation of terminal alkynes catalyzed by low loadings of silver(I)/DMSO at ambient CO_2 pressure.¹⁹ Iwasawa's group reported the direct carboxylation of arenes with CO_2 using rhodium(I)-catalyzed via chelation-assisted C-H bond activation.²⁰ Zhang Yugen et al. have disclosed a copper-NHC-catalyzed transformation of CO_2 to

carboxylic acid through C-H bond activation of terminal alkynes, which was carried out under ambient conditions and tolerant to a wide range of functional groups.²¹ (Scheme 2) In theoretical aspects, some relevant researches have been carried out, such as the carboxylation of arene C-H bond²², arylboronate esters²³, C-H bond of heteroarenes²⁴ with CO_2 catalyzed by metal complexes respectively.



15 **Scheme 3.** The perspective of the three reaction pathways calculated.

With regards to the reaction mechanisms of the carboxylation of terminal alkynes catalyzed by the copper-NHC complexes with CO_2 , it is still unclear. Besides, the roles NHC plays in these reactions are also an interesting and key issue.²⁵ In order to solve the two issues above, the mechanisms of title reaction have been studied by DFT calculations in this study. We designed, explored and compared three types of reaction mechanisms (Scheme 3) and investigated how the additional NHC affects the reaction

25 process. The optimal reaction channels for title reaction were selected out. The transformations of NHC types, which is still a hotspot recently,²⁶ were discussed to help to interpret the differences of the reaction mechanisms. Understanding the reaction mechanisms and the functions of NHC are expected to help to devise more efficient synthetic strategies and more efficient catalysts for carboxylation reactions utilizing CO_2 .

2. COMPUTATIONAL DETAILS

Molecular geometries of the model complexes were optimized without constraints via DFT calculations using the B3LYP²⁷ functional within the Gaussian 09 programs.²⁸ Frequency calculations at the same level of theory have also been performed to identify all of the stationary points as minima or transition states. For the Cu atom, the all-electron split valence basis set 6-311G* Wachters-Hay²⁹ was used. The 6-311G(d,p) basis set was used for all other atoms. Intrinsic reaction coordinates (IRC)³⁰ were calculated for the transition states to confirm that such structures indeed connect two relevant minima. To include

the effect of the solvent on the optimal reaction channels, the conductor-like polarizable continuum model (CPCM)^{31,32} using UAHF radii on it was employed with dimethylformamide (DMF) ($\epsilon = 37.219$) in consideration of the solvent used in experiment. Partial atomic charges were calculated on the basis of natural bond orbital (NBO) analyses³³ and Mulliken charges were used in this study. A large quantity of papers³⁴ had also demonstrated the suitability and the correctness of this DFT method. The charge decomposition analysis is obtained by Aomix³⁵ and Multiwfn³⁶.

We calculated the energies of initial reactant with different conformations and picked out the lowest one, the two branches of whose structure is *trans*- site, was used in our study.

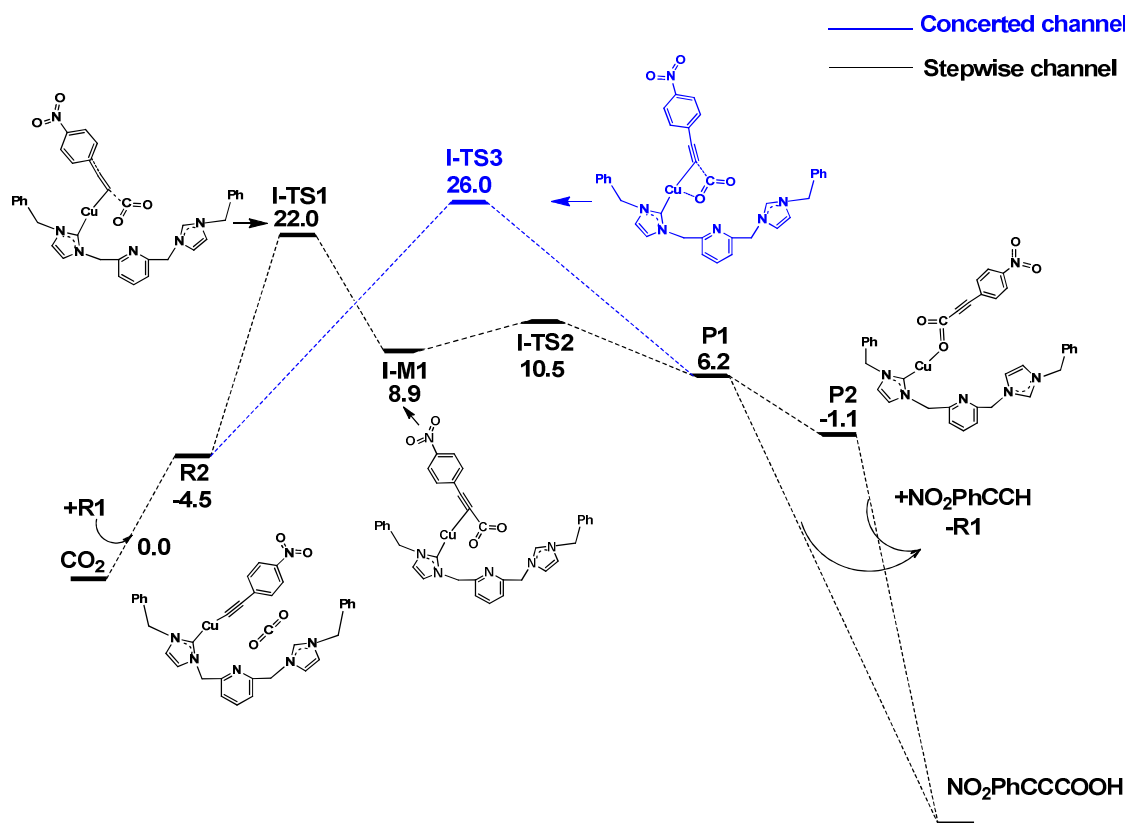


Figure 1. The potential energy profiles of PW-I. All the energies listed are the Gibbs free energies. (kcal mol^{-1}).

3. RESULTS AND DISCUSSION

Pyridine-1-(ethylbenzene-NHC)-5-(ethylbenzene-NHC)-p-nitrobenzene copper acetylide **R1** and its isomeride **III-M1** are generated as the equation shown in Scheme 2. Substituent NO_2 is also a strong electron-withdrawing group, but not a general H substituent, which is helpful for the reaction to continue. Scheme 3 gives out the possible reaction mechanism between them and CO_2 , respectively. Both pathway I (PW-I) and pathway II (PW-II) are catalyzed by **R1** initially. Pathway I is the direct insertion process of CO_2 with two channels, including the concerted and the stepwise channels. Pathway II is the insertion process of activated CO_2 by NHC, with four channels. After the formation of **II-M3**, channels A and B are distinguished from the conformations between copper atom and the two oxygen atoms, (**B-M1** and **A-M2**), while channels C and D can proceed through two-steps and one-step reactions respectively. Pathway III is the insertion process of CO_2 catalyzed by **III-M1** initially,

proceeding through one transition states **III-TS**. In these pathways, **R1** and **III-M1** are all recyclable.

3.1 Pathway I (PW-I): The direct insertion of process of CO_2

The calculated potential energy profiles for the reaction process of the direct carboxylation of 4-nitro-1-ethynylbenzene with CO_2 catalyzed by the copper-NHC complex are shown in Figure 1. As shown in Figure 1, the formation of **R2** lets the sum of Gibbs energy of **R1** and CO_2 drop to $-4.5 \text{ kcal mol}^{-1}$ after the common optimization. The electronic interaction energy between fragment **R1** and fragment CO_2 in their adduct **R2** is $-7.17 \text{ kcal mol}^{-1}$. (Table 1) This is in line with the lowest one during the process, which reveals that the interaction between these two fragments is strengthening gradually. From complex **R2** (Figure S1) to **P1** (Figure S1), two different possible reaction mechanisms for CO_2 insertion into Cu-C bond are considered when CO_2 is catalyzed directly, including the concerted and stepwise channels.

In the concerted channel, CO_2 interacts with both Cu metal

center and the associated C atom synchronously, generating complex **P1** via the transition state **I-TS3** (Figure 2). The energy barrier is 30.5 kcal mol⁻¹.

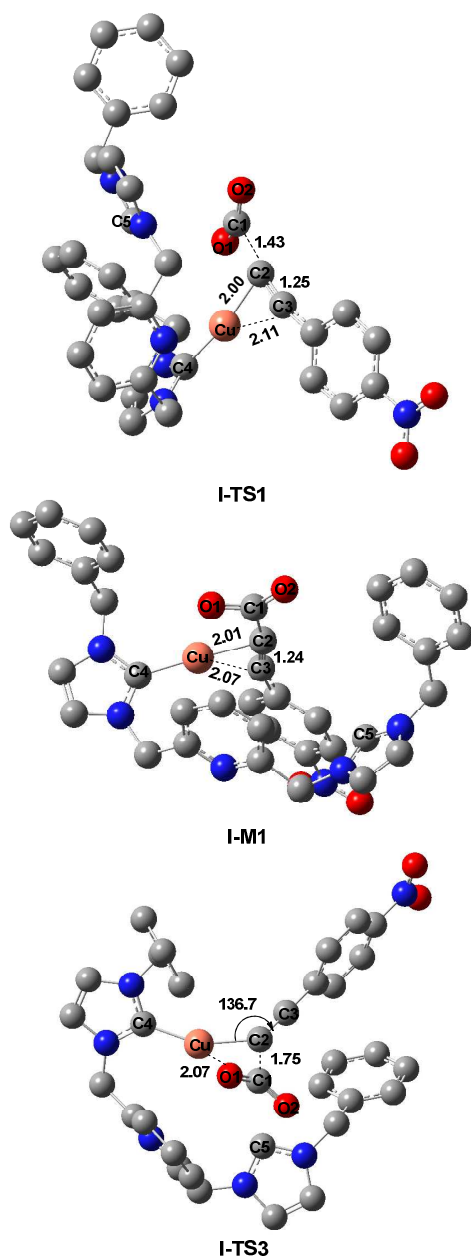


Figure 2. The structures of **I-TS1**, **I-M1**, **I-TS3** in PW-I. All the hydrogen atoms are omitted. The bond distances and bond angles are measured by Å and degree, respectively.

Nevertheless, the stepwise channel has the lower maximum energy barrier of 26.5 kcal mol⁻¹ from complex **R2** to **I-TS1**

(Figure 2), providing an intermediate **I-M1** (Figure 2). The forming of C1-C2 bond occurs firstly and then the Cu-O1 bond forms, accompanied with the breaking of Cu-C2 bond. Since the coordination ability of carboxylate oxygen vs C2-C3 bond π system, with the forming of C1-C2 bond, the bond distance of C2-C3 elongates to 1.25 Å in **I-TS1** first and then has a slight shortening in **I-M1** (1.24 Å). Meanwhile, the Cu-C2 bond distance elongates from 2.00 Å in **I-TS1** to 2.01 Å in **I-M1**. This also results in the Cu-C2-C3 angles in both **I-TS1** and **I-M1** are acute angles, which is different from the corresponding obtuse angles in **I-TS3** of the concerted channel.

Table 1. The charge decomposition analysis of different fragments in the relevant complexes and transition states in PW-I.^A

	$d \times 10^{-3}$	$b \times 10^{-2}$	$(d-b) \times 10^{-2}$	$r \times 10^{-2}$	$E(\text{int}) / \text{kcal mol}^{-1}$
R2					-7.17
I-TS1					- 19.26
HOMO+12	0.044	1.189	-1.182	-1.557	
HOMO+22	1.665	2.981	-2.814	-3.694	
I-M1					- 69.81
HOMO+28	0.985	1.986	-1.887	-2.797	
I-TS2					- 82.26
HOMO+20	9.377	0.388	0.550	0.027	

A: d - the number of electrons donated from fragment $(\text{C}_6\text{H}_5\text{NO}_2)\text{C}\equiv\text{C}(\text{CO}_2)$ to fragment L-Cu; b - the number of electrons back donated from $(\text{C}_6\text{H}_5\text{NO}_2)\text{C}\equiv\text{C}(\text{CO}_2)$ to fragment L-Cu; r - the number of electrons involved in repulsive polarization; $E(\text{int})$ - the electronic interaction energy between fragment R1 and fragment CO_2 .

From stage **I-M1** to **P1**, the energy barrier is small, only 1.6 kcal mol⁻¹. The structure of **I-TS2** is more profitable for the formation of Cu-O1 bond and the weakening of the interaction between Cu atom and $\text{C}\equiv\text{C}$ bond with the strengthen of coordination ability of carboxylate O vs C2-C3 π system. (Table 1 and Figure S3) Meanwhile, the dihedral angle Cu-C2-C1-O1 in **I-TS3** (-40.7°) is larger than that in **I-TS1** (-31.5°), which is also favorable for the concerted interaction between Cu-C2 single bond and O1-C1 double bond.

To sum up, the asynchronous channel is superior to the concerted one. **P1** and **P2** are isomerides. CO_2 is turned into 4-nitro-1-ethynylbenzene acid after the addition of 4-nitro-1-ethynylbenzene and the losing of **R1** finally.

Cite this: DOI: 10.1039/c0xx00000x

www.rsc.org/xxxxxx

ARTICLE TYPE

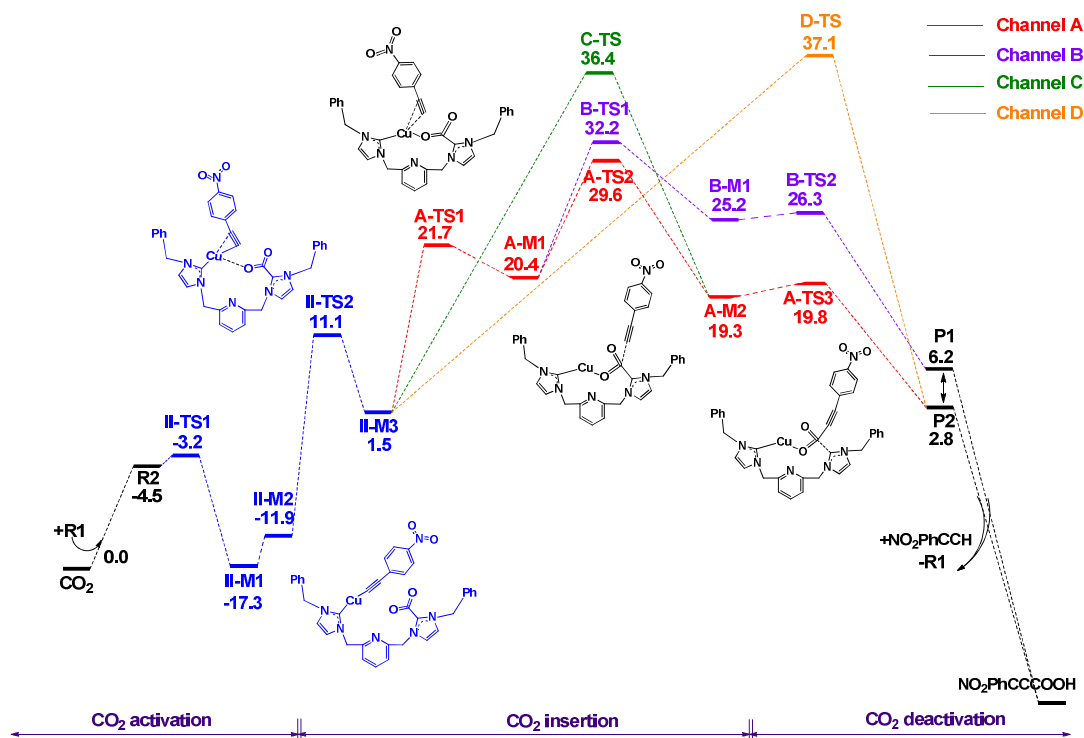


Figure 3. The potential energy profiles of PW-II. All the energies listed are the Gibbs free energies. (kcal mol^{-1}).

3.2 Pathway II (PW-II): the insertion process of activated CO_2 by NHC

As we all know, NHC is an efficient catalyst to activate CO_2 ,^{2a,39} so most of the time, the involved CO_2 is easy to be activated by the free carbene. Figure 3 presents four potential energy profiles of the insertion process of activated CO_2 by NHC, which can be divided into three stages: CO_2 activation, CO_2 insertion and CO_2 deactivation. The CO_2 activation energy barrier required to overcome is only $1.3 \text{ kcal mol}^{-1}$.

After the CO_2 activation by NHC, **II-M1** (Figure 4) is formed. In **II-M1**, one NHC is contributed to form copper-NHC-acetylide, and the other one is contributed to form NHC-activated CO_2 . Due to the strong electrophilicity of copper ($0.602e$) (Table S2), it is easy to attract the adjacent electronegative oxygen atom ($-0.518e$) to generate the VDW complex **II-M2** (Figure S2), heightening the energy barrier a little, about $5.4 \text{ kcal mol}^{-1}$.

Then during the stage of CO_2 insertion, by reference to the charge decomposition analysis results, the electronic interaction energy between fragment **R1** and fragment CO_2 becomes larger and larger, which shows the reaction process between them. (Table S6) It is the strong donation interaction between fragment L-Cu and fragment CO_2 that induces the formation of intermediate **II-M3** (Figure 4) via **II-TS2** (Figure S2), with an energy barrier of $23.0 \text{ kcal mol}^{-1}$. The Cu-O1 distance goes on shortening to 2.47 \AA .

Starting from **II-M3**, four channels were designed and

calculated. Channel A and B will go through the same transition state **A-TS1** (Figure S4) to obtain the intermediate **A-M1** (Figure 4), with $20.2 \text{ kcal mol}^{-1}$ energy barrier. In this step, Cu-O1 bond is formed, along with the disassociation of fragment L-Cu and the acetylide moiety. The bond distance of Cu-O1 shortens to 1.83 \AA in **A-M1** (1.87 \AA in **A-TS1**). The second order perturbation theory analysis shows that Cu-O bond has been formed in **A-TS1**, and the acetylide moiety begins to divorce from copper center. The charge of C3 atom in **A-M1** also decreases largely to $-0.047e$. (Table S2)

From here on out, channel A and B are divided. In channel A, a half-encircled structure complex **A-M2** (Figure S4) is formed via **A-TS2**, with the energy barrier of only $9.2 \text{ kcal mol}^{-1}$. Table S6 shows the strong back donation interaction between fragment L-Cu(CO_2) and fragment $(\text{C}_6\text{H}_5\text{NO}_2)\text{C}\equiv\text{C}$ in HOMO+2 orbital of **A-TS2**, performance on the strong virtual frequency vibration between C1 and C2 atoms. In **A-M2**, the bond distances of Cu and O1 and O2 atoms are 1.88 \AA and 2.05 \AA , respectively.

Until now, CO_2 has been successfully inserted into the metal-carbon bond. Due to the instability of NHC complex, it is so easy to break this C-C bond to vacate this NHC to recover its capacity of activating CO_2 again via **A-TS3** (Figure S4) finally. The energy barrier of this step is very small, only $0.5 \text{ kcal mol}^{-1}$.

For channel B, the similar reaction mechanism is found, except the intermediate **B-M1** (Figure S4) and production **P1** replacing their corresponding isomerides **A-M2** and **P2** in channel A respectively. The Cu-O1-O2 dihedral angle is -24.3°

while that in **B-M1** is 90.3° . That means the acetylide moiety attacks the rest moiety from two different orientations. The energy barrier is also a little higher compared to that of channel A, about $11.8 \text{ kcal mol}^{-1}$.

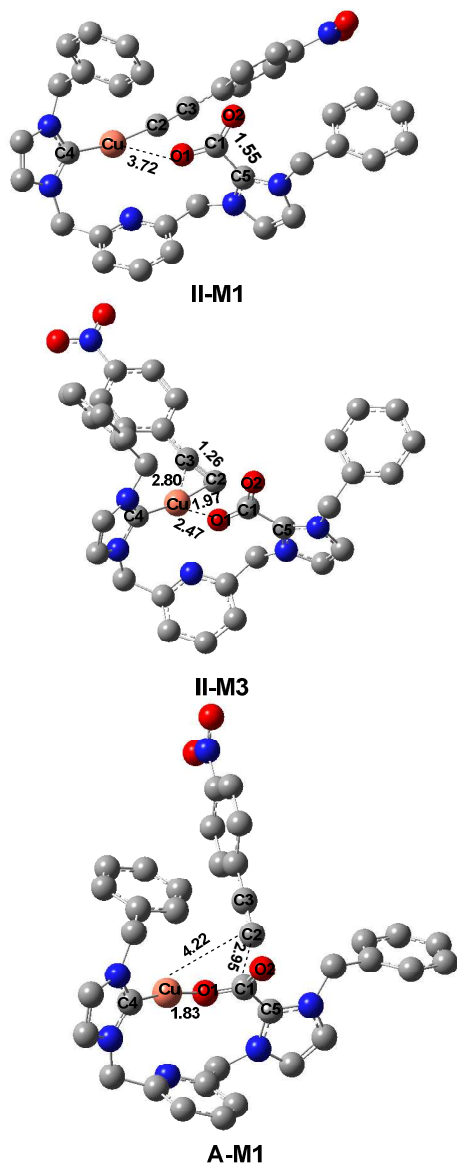


Figure 4. The structures of **II-M2**, **II-M3**, **A-M1** in PW-II. All the hydrogen atoms are omitted. The bond distances and bond angles are measured by Å and degree, respectively.

In channel C, the formations of Cu-O1 and C2-C1 bonds occur synchronously during the process of CO₂ insertion. **A-M2** is generated after a much higher energy barrier of $34.9 \text{ kcal mol}^{-1}$ via **C-TS** (Figure S5). In channel D, the insertion process of CO₂ moiety into Cu-C bond and the process of CO₂ deactivation are realized in one step after **D-TS** (Figure S5), generating the same product **P2**. So channel D has the highest energy barrier of $35.6 \text{ kcal mol}^{-1}$.

Compared with these four possible reaction channels, it is obvious that channel A is optimal. For the reaction mechanism, a

universal speculation is that the transfer of CO₂ unit from the carbene center to copper center²¹ is induced by the formation of new C-C bond. However, our calculations show that, actually, the Cu-O bond is formed firstly, and then inducing the formation of new C-C bond to finish the transfer of CO₂.

It is worth noting that the reaction process is indeed promoted after the formation of CO₂-NHC-Cu cocatalyst (**II-M2**), corresponding to the lower maximum energy barrier needed to overcome. On the contrary, because the energy of CO₂-NHC-Cu cocatalyst is much smaller, this situation instead makes a negative effect for the whole reaction process.

3.3 Pathway III (PW-III): the insertion process of CO₂ catalyzed by **III-M1** initially

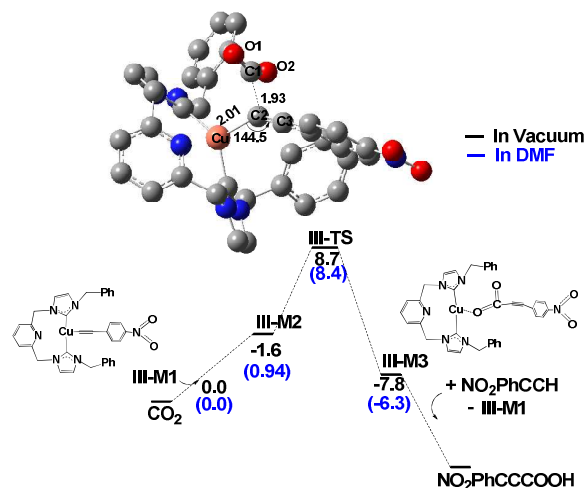


Figure 5. The potential energy profiles of PW-III. (kcal mol⁻¹) For the structure of **III-TS**, all the hydrogen atoms are omitted. The bond distances and bond angles are measured by Å and degree, respectively. All the energies listed are the Gibbs free energies.

In PW-II, it is obvious that the reaction process is promoted after the formation of CO₂-NHC-Cu cocatalyst. Then, what will an associative path in which the NHC fragment acts as bidentate ligand happen? Therefore, pathway III is investigated. Herein, the energy of starting reactant **III-M1**, the structure containing two NHCs connected by the same Cu metal center, is $11.2 \text{ kcal mol}^{-1}$ lower than that of its isomeride **R1**. Also, an interesting phenomenon was found during this calculation. It is, the largest energy barrier of this classical associative pathway is much lower than that of PW-I and PW-II, only $10.3 \text{ kcal mol}^{-1}$. C1 and C2 atoms in **III-TS** (Figure 5) have a strong interaction to form bond, with the charges of $0.543e$ and $-0.634e$, respectively. (Table S4) From **III-M2** (Figure S6) to **III-TS**, the C1-C2 distance shortens largely from 3.32 Å to 1.93 Å . This interaction motivates the reaction to go further and gives a chance for Cu atom to interact with O1 atom deserved. In **III-M3** (Figure S6), the distance of Cu-O1 elongates to 2.14 Å . Cu-O1-C1-O2 atoms can only form a half-encircled structure due to the steric hindrance of chelation. The distances of Cu-O1 and Cu-O2 bonds are 2.14 Å and 3.14 Å , respectively.

Cite this: DOI: 10.1039/c0xx00000x

www.rsc.org/xxxxxx

ARTICLE TYPE

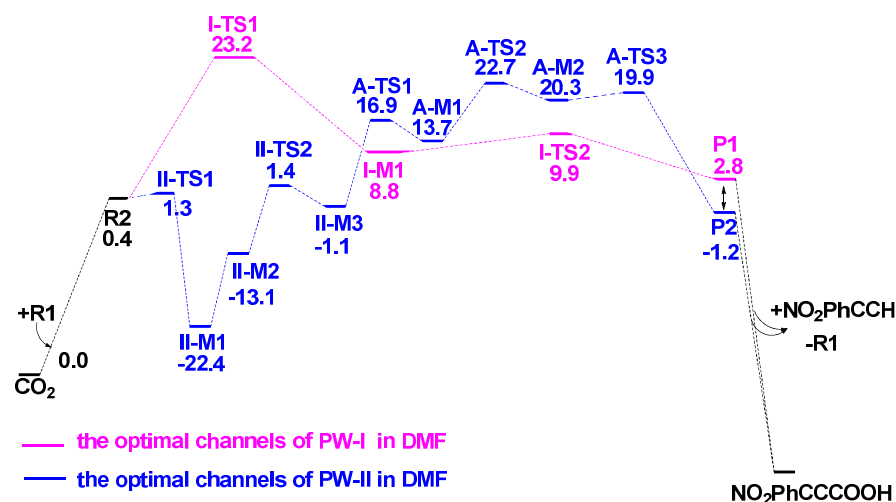


Figure 6. Potential energy profiles of the optimal channels of PW-I and PW-II in DMF. All the energies listed are the Gibbs free energies. (kcal mol^{-1}).

3. 4 DMF solvent effect

DMF solvent effect are considered and added to the optimal channels of these three pathways, (Figure 5 and Figure 6) and then their maximum energy barriers of each steps are compared. In Figure 6, it is found that the maximum energy barrier among each elementary reaction of stepwise channel (optimal channel in PW-I) ($23.2 \text{ kcal mol}^{-1}$) is still smaller than that of channel A (optimal channel in PW-II) ($23.8 \text{ kcal mol}^{-1}$). This result is consistent with that in gas phase. Similarly, the potential energy profile of PW-III in DMF is shown in Figure 5. The sum relative energies of **III-M1** and CO_2 in DMF ($-0.9 \text{ kcal mol}^{-1}$) is a little lower than that in gas phase ($1.6 \text{ kcal mol}^{-1}$), maybe because of the steric hindrance of chelate.⁴⁰ Seemingly, this DMF solvent situation is more helpful for the reaction process actually.

3.5 The roles of NHC

3.5.1 Compared with pathway I and II

In order to explore the role of NHC, the reaction mechanisms of PW-I and PW-II are compared firstly. It is demonstrated that NHC plays a dual role in PW-II, not only to be used to form NHC-Cu cocatalyst as both the ligand and catalyst, but also used as an activating catalyst to activate CO_2 .

The charge decomposition analysis (CDA) and extended CDA (ECDA) were analyzed. (Table 2) The ECDA results show that the total net electrons always transfer from fragment NHC-included to fragment copper-included, which is one of the typical characters of Fischer-type.⁴¹ However, the carbon atom of Fischer-type NHC linked to Cu center always positively charged, which is not consistent with the Mulliken charges analysis. (Table S5) Analyzing the Mulliken charges changes of the optimal channel of PW-I and PW-II, it is found that the Mulliken charges of carbon atom of NHC change from positive to negative three times totally, which should not be the typical character of

³⁵ Fischer-type.

Table 2. The CDA and ECDA analysis of related complexes and transition states in PW-I and PW-II.

	Complex /Transition state	Net electrons transfer ^A	d_{max} MO number ^B	d_{max}^B
PW-I	R2	0.1368	HOMO+22	0.0443
	I-TS1	0.1055	HOMO+22	0.0199
	I-M1	0.1303	HOMO+1	0.0312
	II-M2	0.0782	HOMO+20	0.0310
PW-II	II-TS2	0.0423	HOMO+2	0.0206
	II-M3	0.0306	HOMO+7	0.0277
	A-TS1	0.5668	HOMO+15	0.0145

A: For PW-I, the net electrons transfer is between $(\text{C}_6\text{H}_5\text{NO}_2)\text{C}\equiv\text{C}-\text{Cu}(\text{CO}_2)$ to fragment L; For PW-II, the net electrons transfer is between $\text{L}-\text{CO}_2$ and $(\text{C}_6\text{H}_5\text{NO}_2)\text{C}\equiv\text{CCu}$. B: d_{max} is the max number of electrons donated from fragment NHC-included to fragment of copper-included among all MO.

So the orbital diagrams donated maximum electrons number was compared. (Figure S8 and Figure 7) It is found that all the orbital diagrams of complex and transition states charge changed into negative (**I-M1**, **II-TS2** and **A-TS1**) don't reveal the corresponding Fischer-type shape. In Figure S7 and Figure 7, the d_{max} orbital diagrams of **R2**, **I-TS1**, **II-M2** and **II-M3** illustrate that their NHCs are all the typical Fischer-type. (Figure 7) However, for **II-TS2** and **A-TS1**, they show approximate temporary Schorck-type⁴² shape NHCs, while for **I-M1**, it shows the approximate σ bond shape. (Figure 7)

These abnormal phenomena result in the different reaction activity of NHC linked to copper center. Meanwhile, we can find the energy barrier from **II-M3** to **A-TS1** in PW-II ($20.2 \text{ kcal mol}^{-1}$) is lower than that from **R2** to **I-TS1** in PW-I ($26.5 \text{ kcal mol}^{-1}$) in gas phase. This shows that CO_2 activated by NHC can really

promote the reaction process after the formation of CO₂-NHC-Cu cocatalyst. However, due to the dramatically dropping of the energy of the cocatalyst **II-M1**, the maximum energy barrier of elementary reactions in PW-II becomes to 28.4 kcal mol⁻¹ (from **II-M1** to **II-TS2**), which is larger than that in PW-I. Therefore, this abnormal overstable activated CO₂-NHC-Cu cocatalyst results in the maximum energy barriers of the total reaction process increasing but not decreasing in PW-II finally.

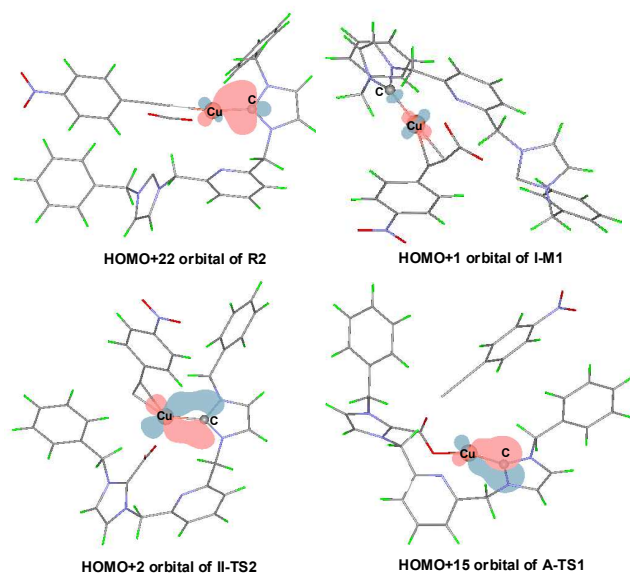


Figure 7. The d_{\max} orbital diagrams of related complexes and transition states in PW-I and PW-II. (the part of C atom of NHC and Cu atom that it linked)

3.5.2 Compared with pathway I and III

For the direct CO₂ insertion processes, the reaction energy barrier of PW-III is much lower than that of PW-I. It is obviously that PW-III has much higher reaction activity than that of PW-I. So what role does NHC play here?

The two catalysts of PW-I and PW-III (**R1** and **III-M1**) have different structures. **R1** is a chelate via one pyridine ring associated two NHCs, with only half of the carbene species coordinated with copper, the other half remained free carbenes. While in **III-M1**, two NHCs are associated with the same copper center. This can be great helpful for increasing the electropositivity of Cu (from 0.534e in **R1** to 0.841e in **III-M1**) in PW-III.

Based on the NBO calculations, we compared the second-order stabilization energy 'E(2)' of key stationary points (SP) in the two pathways. For PW-I, C4 atom of NHC always has a strong interaction to donate its lone pair electrons to the unoccupied orbital of Cu atom in **R2**, **I-TS1**, **I-TS3**, with the relative big "E(2)" values (64.3, 59.7, 54.7 kcal mol⁻¹). (Table S1) Taking **I-TS1** as an example, the orbital imagery of the favorable NBO donor-acceptor interactions of LP(C4) → LP*(Cu) in **I-TS1** is shown in Figure 8.⁴¹ Similarly, for PW-III, the LP(C4) → LP*(Cu), LP(C5) → LP*(Cu) interactions are both always responsible for the high degree of electron delocalization (Table 3) in all corresponding relevant complexes and transition states.

To sum up, the additional interaction of NHC to the same

metal atom increases the electrophilic of the metal center. This special design promotes the reaction process greatly. This is the reason why PW-III is the optimal pathway.

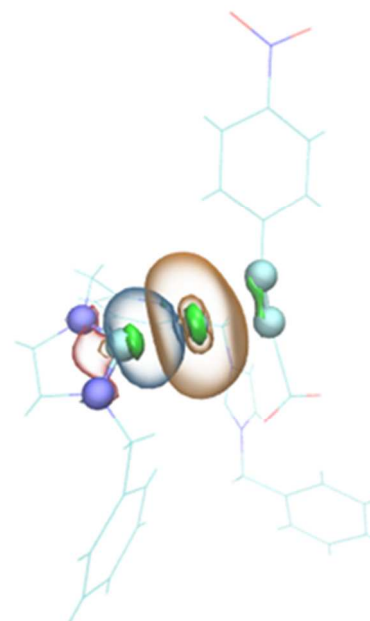


Figure 8. The orbital imagery of the favorable NBO donor-acceptor interactions of LP(C4) → LP*(Cu) in **I-TS1**. Blue and red represent the plus and minus isosurfaces of LP(C4), respectively; Orange and green represent the plus and minus isosurfaces of LP*(Cu), respectively.

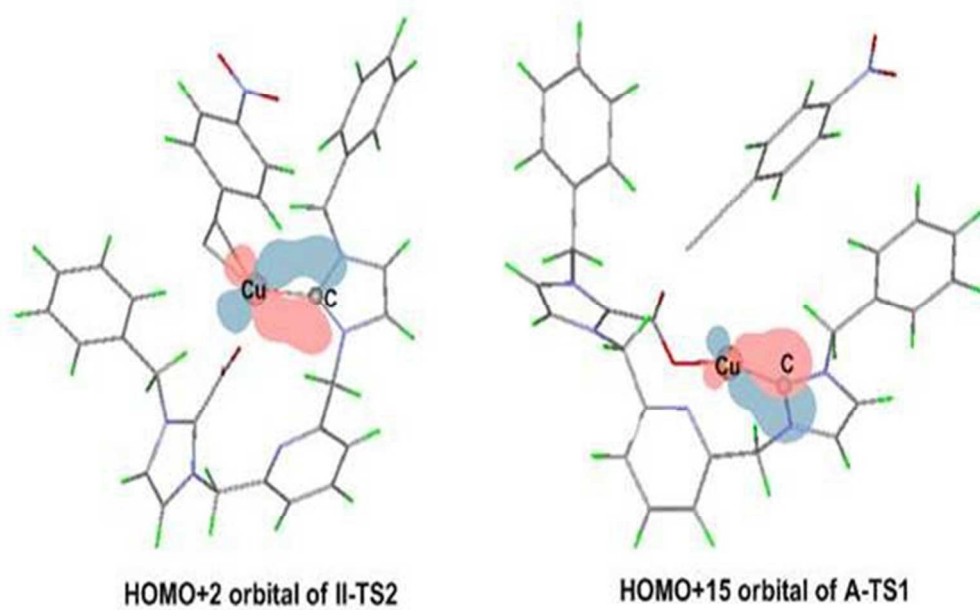
4. Conclusions

In conclusion, DFT calculations had been carried out to study the reaction mechanisms of C-H carboxylation of terminal alkynes with CO₂ by copper(I)-NHC complexes. Three types of reaction mechanisms were explored and compared. For the direct insertion process of CO₂ starting from **R1**, the asynchronous channel is superior to the concerted channel. For the insertion process of activated CO₂ by NHC, four channels were calculated and channel A was selected as the optimal one. Also, the functions of NHC were figured out to help to get insight into how NHC influences the reaction process. The insertion process of CO₂ starting from **III-M1** was also designed to auxiliary assist the research of the role of NHC.

For the reaction mechanisms, an unexpected finding is that an abnormal ultrastable cocatalyst with quite low energy is generated in the insertion process of activated CO₂ by NHC, which is one of the main reasons to increase the difficulty of the energy barriers' dropping in the whole reaction of PW-II, even though the special difunctional roles of NHC (not only to be used to form NHC-Cu cocatalyst as both ligand and catalyst, but also used as an activating catalyst to activate CO₂) can indeed facilitate the reaction process after its generation actually. Also, the Mulliken charges of carbon atom of NHC change from positive to negative three times totally, which indicates this NHC is not a typical Fischer-type carbene in the reaction process actually. Compared to the experimental proposed mechanism, in PW-II, we also found that the formation of new C-C bond was induced by the formation of Cu-O bond, but not the formation of new C-C bond as the universal speculation. Besides, the

26. *Organometallic Oxidation Catalysis* in Topics in Organometallic Chemistry; F. Meyer, C. Limberg, Springer, 2007.
27. (a) C. T. Lee, W. T. Yang, R. G. Parr, *Phys. Rev. B* **1988**, 37, 785. (b) A. D. Becke, *J. Chem. Phys.* **1993**, 98, 5648. (c) B. Miehlich, A. Savin, H. Stoll, H. Preuss, *Chem. Phys. Lett.* **1989**, 157, 200.
28. Gaussian 09, Revision A02, M. J. Frisch, G. W. Trucks, H. B. Schlegel, G. E. Scuseria, M. A. Robb, J. R. Cheeseman, G. Scalmani, V. Barone, B. Mennucci, G. A. Petersson, H. Nakatsuji, M. Caricato, X. Li, H. P. Hratchian, A. F. Izmaylov, J. Bloino, G. Zheng, J. L. Sonnenberg, M. Hada, M. Ehara, K. Toyota, R. Fukuda, J. Hasegawa, M. Ishida, T. Nakajima, Y. Honda, O. Kitao, H. Nakai, T. Vreven, J. A. Montgomery, Jr., J. E. Peralta, F. Ogliaro, M. Bearpark, J. J. Heyd, E. Brothers, K. N. Kudin, V. N. Staroverov, T. Keith, R. Kobayashi, J. Normand, K. Raghavachari, A. Rendell, J. C. Burant, S. S. Iyengar, J. Tomasi, M. Cossi, N. Rega, J. M. Millam, M. Klene, J. E. Knox, J. B. Cross, V. Bakken, C. Adamo, J. Jaramillo, R. Gomperts, R. E. Stratmann, O. Yazyev, A. J. Austin, R. Cammi, C. Pomelli, J. W. Ochterski, R. L. Martin, K. Morokuma, V. G. Zakrzewski, G. A. Voth, P. Salvador, J. J. Dannenberg, S. Dapprich, A. D. Daniels, O. Farkas, J. B. Foresman, J. V. Ortiz, J. Cioslowski and D. J. Fox, Gaussian 09, Wallingford CT, **2009**.
29. (a) A. J. H. Wachters, *J. Chem. Phys.* **1970**, 52, 1033. (b) P. J. Hay, *J. Chem. Phys.* **1977**, 66, 4377.
30. (a) K. Fukui, *J. Phys. Chem.* **1970**, 74, 4161. (b) K. Fukui, *Acc. Chem. Res.* **1981**, 14, 363.
31. V. Barone, M. Cossi, *J. Phys. Chem. A* **1998**, 102, 1995.
32. M. Cossi, N. Rega, G. Scalmani, V. Barone, *J. Comput. Chem.* **2003**, 24, 669.
33. (a) A. E. Reed, L. A. Curtiss, F. Weinhold, *Chem. Rev.* **1988**, 88, 849. (c) Foster, J. P.; Weinhold, F. *J. Am. Chem. Soc.* **1980**, 102, 7211.
34. (a) C. H. Suresh, M. J. Ajitha, *J. Org. Chem.* **2013**, 78(8), 3918–3924. (b) J. J. Lippestreu, B. F. Straub, *J. Am. Chem. Soc.* **2005**, 127(20), 7444. (c) H. Jacobsen, A. Correa, A. Poater, C. Costabile, L. Cavallo, *Coord. Chem. Rev.* **2009**, 253(5-6), 687. (d) G. Frison, A. Sevin, *J. Phys. Chem. A* **1999**, 103(50), 10998. (e) A. R. Rod, E. Vessally, *Asian J. Chem.* **2007**, 19(3), 1709. (f) C. Trindle, *J. Org. Chem.* **2003**, 68(25), 9669.
35. I. Hypercube, Hypercube Inc., USA, HyperChem 8.0, 2007
36. T. Lu. Multiwfn, version 2.4; <http://multiwfn.codeplex.com>.
37. H. Lang, A. Jakob, B. Milde, *Organometallics* **2012**, 31(22), 7661–7693.
38. M. S. Nechaev, V. M. Rayon, G. Frenking, *J. Phys. Chem. A* **2004**, 108(15), 3134–3142.
39. L. Q. Gu, Y. G. Zhang, *J. Am. Chem. Soc.* **2010**, 132(3), 914.
40. X. H. Liu, R. Pattacini, P. Deglmann, P. Braunstein, *Organometallics* **2011**, 30(12), 3302–3310.
41. E. O. Fischer, A. Maasbol, *Angew. Chem. Int. Ed. Engl.* **1964**, 3, 58.
42. R. R. Schrock, *Accts. Chem. Rev.* **1979**, 12, 98.

50



131x64mm (116 x 150 DPI)